Journal of Colloid and Interface Science 449 (2015) 92–101

Contents lists available at ScienceDirect

Journal of Colloid and Interface Science

www.elsevier.com/locate/jcis

The dynamics of capillary-driven two-phase flow: The role of nanofluid structural forces

Alex Nikolov *, Hua Zhang

Department of Chemical and Biological Engineering, Illinois Institute of Technology Chicago, 10 West 33rd Street, Chicago, IL 60616, United States

ARTICLE INFO

Article history:
Received 10 September 2014
Accepted 18 October 2014
Available online 5 November 2014

Keywords:
Capillary-driven flow
Nanofluid
Self-layered
Structural forces
Oil displacement

ABSTRACT

Capillary-driven flows are fundamental phenomena and are involved in many key technological processes, such as oil recovery through porous rocks, ink-jet printing, the bubble dynamics in a capillary, microfluidic devices and labs on chips. Here, we discuss and propose a model for the oil displacement dynamics from the capillary by the nanofluid (which is composed of a liquid suspension of nanoparticles); we elucidate the physics of the novelty of the phenomenon and its application. The oil displacement by the nanofluid flow is a multi-stage phenomenon, first leading to the oil film formation on the capillary wall, its break-up, and retraction over the capillary wall; this lead to the formation of the oil double concave meniscus. With time, the process repeats itself, leading to the formation of a regular "necklace" of oil droplets inside the capillary. Finally, the oil droplets are separated by the nanofluid film from the capillary wall. The light reflected differential interferometry technique is applied to investigate the nanofluid interactions with the glass wall. We find nanoparticles tend to self-structure into multiple layers close to the solid wall, which cause the structural forces to arise that lead to the oil displacement from the capillary. This research is expected to benefit the understanding of nanofluid phenomena in a capillary and promote their use in technological applications.

1. Introduction

We would like to dedicate this work to Professor D.T. Wasan, a remarkable person who has made outstanding contributions to colloid and interface science and their technological applications and puts science to work. Eli Ruckenstein of SUNY Buffalo once described Darsh Wasan as an "imaginative experimentalist, a versatile theoretician and man with technological insight". His interests and contributions to nano-colloid science and technology are amazingly diverse. It is not easy to summarize his achievements and his contributions, because over the course of his 50-year professional career, his research has spanned a number of interrelated fields. His work has affected important areas such as surface/interfacial rheology, liquid film dynamics and the stability of foams and emulsions, the nanofluid film structuring phenomenon, and the role of structural forces on the wetting and spreading of nanofluids on solids.

Capillary-driven flows are fundamental phenomena elucidating multiple phases of flow inside the capillary. The multiphase flow in capillaries and porous media is a topic of great scientific and technological interest. It would be an overwhelming task to review all the research in this area, so here we will only briefly present the most relevant research concerning the capillary-driven flow and discuss the role of the nanofluid's structural forces. Lucas [1], Washburn [2] and Rideal [3] studied the meniscus dynamics of a simple fluid in a capillary. Bretherton [4] examined the bubble dynamics in a tube. The flow of soluble dispersions in capillaries was elucidated by Griffiths [5], Taylor [6,7], Goldman et al. [8], Frankel and Brenner [9], Brenner and Edwards [10], and Dorfman and Brenner [11]. Recently, there has been an increased focus on the flow dynamics of simple fluids in nanotubes with structured walls [12–15].

In this research, we examine the flow dynamics of a nanofluid (complex fluid) under capillary confinement and elucidate the role of the structural forces for phase separation and the fabrication of dispersions and microfluidic devices.

The goal of the presented research is to examine the role of the nanofluid (e.g., two-phase dispersion) on the phase displacement–separation phenomena as it moves slowly (small capillary number) in a capillary filled with the oil phase. In order to elucidate the role of the capillary wall on the flow dynamics, we will briefly discuss the fundamental phenomena related to two-phase flows in the capillary. The research behind the two-phase and multiphase flows in a capillary has an intriguing history. The research of the flow in a

* Corresponding author. Fax: +1 312 567 3003.
E-mail address: nikolov@iit.edu (A. Nikolov).

http://dx.doi.org/10.1016/j.jcis.2014.10.057
0021-9797/

capillary has focused on the meniscus dynamics (Lucas–Washburn–Rideal (LWR)) and fluid velocity profile in a tube (first, Griffiths in 1910 [5], then Taylor in 1953 [6], and later Brenner et al. [9,10]). Griffiths [5] found experimentally that the aqueous solution with coloring matter (fluorescent dye) spreads out in a symmetrical manner from a point which moves with the mean velocity of the water in the tube. Taylor [6,7] concluded that the soluble dispersion in a steady flow is due to the combined action of the convection parallel to the axis and molecular diffusion in the radial direction. Brenner and other researchers [9,10] discussed the Taylor "dispersion phenomena"; they proposed a general theory of the convective-diffusion of Brownian solute particles and applied this theory to microfluidic and sedimentation systems [11]. The importance of Taylor's research on dispersions (or Brownian solute particles) can be seen in the way the nanofluid and/or macromolecule behaves as Brownian solutes disperse in a solvent: the wall effect of the capillary wall confines the nanoparticle or macromolecule, since these tend to layer at the wall [16–20] and impact the fluid flow dynamics. In the event of a bubble/droplet moving in a capillary filled with a nanofluid, the nanofilm structure formed between the bubble/droplet and capillary impacts the bubble/droplet rate of flowing. Bretherton [4] studied the long bubble movement dynamics in horizontal and vertical tubes filled with a single Newtonian fluid (in the case of low capillary numbers) and considered the role of the wetting film between the bubbles. He assumed the forces on the bubble are those due to the viscosity, capillary forces, and gravity. Based on the lubrication approach, he proposed an asymptotic equation for the bubble velocity. The validity of the Bretherton equation was verified by Marchessault and Mason [21] and Goldsmith and Mason [22]. Bretherton [4] did not elucidate the wetting film's bubble/tube wall properties such as the thickness, structure, and stability. He assumed that for the bubble to flow into the tube, the wetting film's bubble has to be stable. What maintains the wetting film's stability? What is the contribution of the nanofluid? These questions were our inspiration to conduct research on the role of the nano-dispersion on the fluid dynamics in a capillary. The film's thickness and ability to wet a wall, its structure and stability are known in the literature as the "coating flow" and has been the subject of many long discussions [23–27]. Landau and Levich [23] proposed that the final film thickness is small compared with the overall length scale of the flow field when the capillary number is small. The film steady-state thickness that Landau–Levich proposed assumed that if the film thickness is much less than the static meniscus-film curvature, the coated film thickness is proportional to the capillary number $(Ca)^{2/3}$ and film–meniscus curvature $(1/R)$. The coefficient of the proportionality of the rate vs. capillary number and film meniscus curvature was discussed by Landau and Levich [23], Levich [24], Derjaguin and Levi [25] and also reviewed by Ruschak [27]. The value of the coefficient of proportionality is subject to how the free surface of the wetting film approaches the meniscus' free surface. Landau and Levich [23] found that if the meniscus static curvature in the film-entrainment region is of the order $1/R$ where the two surface regions overlap, then the two regions will blend together. They proposed the value of 1.34 for the coefficient of proportionality. The value of the coefficient also depends on the presence of a surfactant.

The coating models did not discuss what governs the stability of the wetting film. When the fluid meniscus separating the two fluid phases is moving over the wall, the thickness of the coating film is usually of the magnitude of several microns. The stability of the non-draining, micron-thick, wetting, charge–neutral film is the subject of the surface fluctuation that leads to its instability and causes it to break into droplets. In the case of the film meniscus wetting a capillary, the wetting film breaks after some time and retreats over the wall's surface into double concave meniscuses [28]. The phenomenon of the wetting film break-up is usually attributed to the Rayleigh–Taylor instability. Gravity tends to deform the wetting film's free surface when the capillary force tends to restore the deformation; on the film's free surface, fluctuating waves appear to promote the thickness fluctuation. Over time, the amplitude of the one of the wave's lengths becomes dominant and leads to the film's instability and rupture (see [29] Chapter 10, [30] Chapter 5 and [31] Chapter 2).

Another model proposed for a thin film's instability which does not consider the effect of gravity was proposed by Frumkin [32] and Derjaguin [33]. They proposed a theoretical model for a film wetting–dewetting a solid that took into consideration the magnitude of the surface forces vs. film thickness by the disjoining pressure vs. film thickness isotherm. The stability of the film on a solid was proposed based on the concept of Scheludko [34] and Vrij [35] for a suspended free film (e.g., foam film). The wetting film destabilizing mechanism was attributed to the local imbalance between the surface capillary waves vs. film surface forces (e.g., van der Waals or hydrophobic forces), leading to the critical film thickness that triggers the dewetting. Dewetting begins when the film is so thin that the rate of the growth in the fluctuation in the local area is faster than the rate of film thinning. The proposed model predicts that the stability of the film is governed by the stability criteria: $d\Pi/dh$ (the derivative of the disjoining pressure vs. film thickness) and $P_\gamma > \Pi$ (the capillary pressure is larger than the disjoining pressure; see [36] Chapter 12). It is useful to note that the nanofluid wetting the solid and the film stability are governed by the film area rather than the capillary pressure [37]. It was already demonstrated that nanoparticles under the film surface confinement tended to self-structure into multiple 2D layers. Moreover, the particle 2D inlayer structure was of two types: for the layers at the film surfaces, it was 2D cubic or hexagonal while the inner layers were random. The film's free energy and disjoining pressure vs. film thickness decay in an oscillatory fashion. Modeling the instability of the wetting film—when considering the film's molecular structure evolutes vs. its thickness—requires revisiting the commonly accepted wetting and dewetting models. Fig. 1 shows the dimensionless film free energy and disjoining pressure per unit area vs. film thickness scaled by the particle diameter for the effective volume 30 v%. The calculations were performed using the hard sphere potential of interactions, both those between particles as well as those between the particles and film walls. Due to the film confinement effect, both the film's free energy and disjoining pressure vs. the thickness have an oscillatory decay profile, manifesting the role of the structural and depletion forces [16].

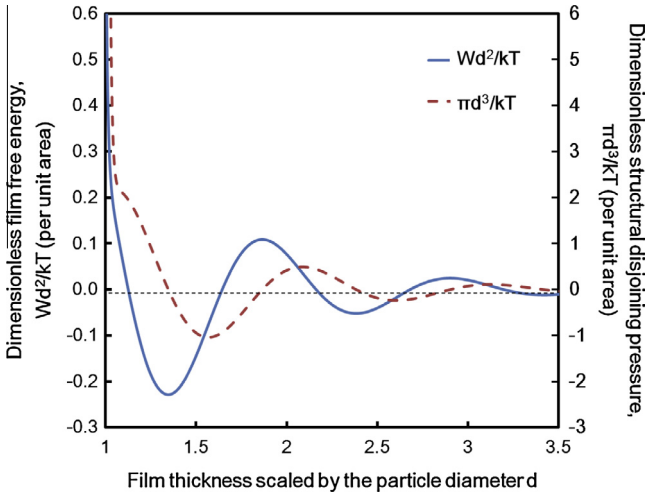

Fig. 1. Dimensionless film free energy and disjoining pressure per unit area vs. film thickness scaled by the particle diameter for the effective volume 30 v%. [37].

The stability of nanofilms wetting solids is due to the fact that nanoparticles in the film tend to self-structure into multiple layers parallel to the solid wall; as a result, the film reduces its thickness in a stepwise manner by stratification, manifesting the particle layering. The particles layered into 2D layers are not perfectly packed and this is especially true for the layers far away from the wall that are less organized and replete with vacancies (free spaces between the particles). The vacancies randomly distributed inside the particle layers that reduce the film's free energy tend to condense, forming a 2D area inside the wetting film with one less particle layer of thickness [38]. Here, we briefly discuss the mechanism of oil displacement by a nanofluid.

Commonly, discussions in the literature concerning the stability of a film wetting a capillary consider the role of the capillary pressure that drives the film to thin [29,30,39–43]. The wetting film in this study is an oil film and is in contact with an oily meniscus with a concave shape. The meniscus capillary pressure drives the wetting film on the capillary wall to thin faster, and as soon as the film reaches its critical thickness, it becomes unstable, ruptures, and forms a double concave meniscus across the capillary wall. The wall of the capillary and the surface's oil double concave meniscus are in contact with the nanofluid. As mentioned earlier, the nanofluid in contact with the wall tends to self-layer. The nanofluid layering promotes its spreading on the wall and enhances the displacement of the oily phase from the capillary wall (Fig. 2).

The objectives of this work are to reveal the detailed mechanisms of the phenomenon in which the nanofluid flow in the capillary comes in contact with the oil phase and promotes nanoparticle self-layering and to examine which structural forces lead to the oil displacement from the capillary. This research is expected to benefit the understanding of nanofluid wetting and spreading phenomena in a capillary and promote their use in technological applications.

Here, we discuss the oil displacement from the capillary by the nanofluid flow; we elucidate the physics of the novelty of the phenomenon and its application. The oil displacement by nanofluid flow is a multi-stage phenomenon: first the oil film forms on the capillary wall, it breaks up, and retracts over the capillary wall, leading to the formation of the oil double concave meniscus; this meniscus separates from the wall and an oil droplet forms. With time, the process repeats itself, leading to the formation of a regular "necklace" of oil droplets inside the capillary that are separated by the nanofluid film from the capillary wall. The photo posted in Fig. 2 depicts the last stage of the phenomenon—oil droplet separation from the wall of the capillary by the nanofluid.

In order to explain the phenomenon of the oil droplet separation from the capillary wall, the following questions need to be answered:

What is the mechanism of the oil displacement from the capillary by the nanofluid that promotes the oil droplet "necklace" phenomenon? Is this specific to the present nanofluid?

To answer these questions, we need to address how the nanofluid interacts with the capillary wall. The nanofluid interactions with the wall that lead to particle layering and 2D in-layering have been studied by Dr. Wasan's group experimentally and by computer modeling [44–50].

2. Experimental

2.1. Review of the experimental techniques for the visual observation of the meniscus

For the capillary-driven flow inside of a cylindrical geometry, it is important to monitor the meniscus profile and understand the interactions of the meniscus and wall since it directly reflects the wettability of the fluid. In general, there are two main approaches, macroscopic and microscopic, that are used to monitor the dynamics of the meniscus.

The macroscopic approach, commonly used in the literature, gives the meniscus profile but it cannot provide much information on how the meniscus interacts with the wall. Methods like the optical technique, pore model, and the coating technique are some examples of this.

The optical technique [28,51–57] is the most frequently used when monitoring the meniscus dynamics. A dye and tracer are used to increase the contrast and better visualize the meniscus movement. Zhang et al. [28] used a red dye soluble in oil and directly monitored the oil film dewetting dynamics inside a glass capillary by transmitted light microscopy. Cachile et al. [51] used a radioactive tracer technique to determine the residual film thickness profile along the length of the tube. Sung et al. [52] investigated the dynamics of a liquid driven by the capillary force in a circular tube and fluorescence microscopy was used to visualize the meniscus movement. Typically, optical techniques for visualizing the meniscus between the texture asperities are limited by either time resolution, or substrate transparency, or both [57].

The two-dimensional (2D) pore model is the simplest technique for monitoring the meniscus in a confined geometry. The 2D pore model is usually designed to mimic oil trapped in a reservoir, allowing for the observation of the oil removal dynamics. Our 2D model was prepared using two flat, rectangular, optically smooth surfaces and magnets (Fig. 3a). The strength of the magnets could be used to change the gap between the surfaces of the 2D pore. The advantage of this technique is that it is simple and can directly visualize the displacement process (Fig. 3b); the disadvantage also lies in its simplicity, as it cannot fully mimic the displacement process in real pores.

The coating technique [23,25] is able to identify how the meniscus interacts based on the reflected light. Fig. 4 shows the climbing film with different layers of silica nanoparticles (the nominal diameter is 20 nm) in it on a silica wafer. The different color bands in the picture indicate different numbers of layers of nanoparticles inside the film.

The microscopic approach can provide information of both the meniscus profile and how the meniscus interacts with the wall.

The reflected light differential interferometry (DI) technique is a microscopic method. It is often used to quantify the thickness of the film and contact angle between the film and meniscus on the solid [46,58–63]. The basic principle is to create interferences between the initial wave front and its copy, which is laterally shifted of a small quantity. The information from the interferogram relates to the wave front derivative in the lateral shift direction, so it is linked to the wave front's slope in the shift direction. Fig. 5

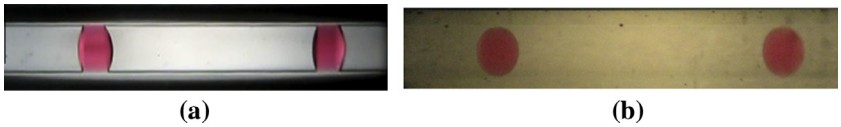

Fig. 2. (a) Oil drops are formed along the capillary wall; (b) oil drops are displaced from the wall by the nanofluid.

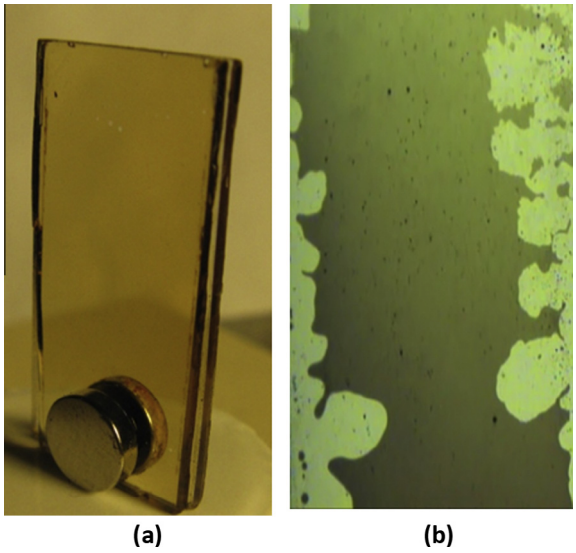

Fig. 3. (a) 2D glass pore model with a uniform oil film between the two slides; (b) crude oil displacement from the 2D glass pore model using a nanofluid.

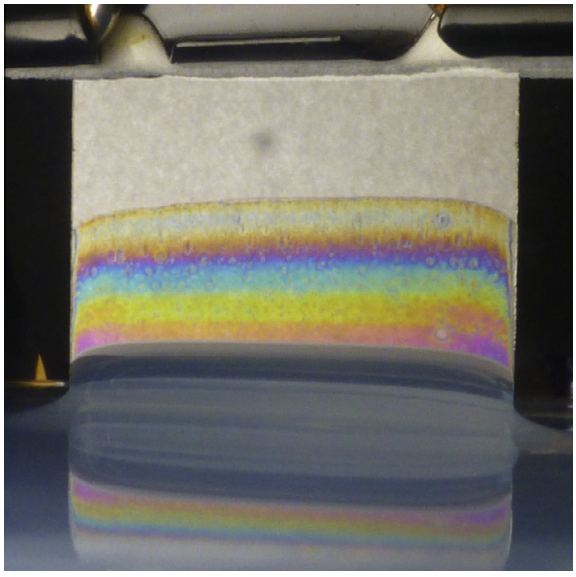

Fig. 4. The climbing film with layers of silica nanoparticles on a silica wafer.

shows a typical the interferogram obtained using differential interferometry.

These techniques have been applied in past for studying moving fluids, but they are also adaptable for nanofluids.

In this study, we used both transmitted light microscope and differential interferometry techniques. The transmitted light microscope was used to monitor the oil meniscus dynamics inside of a transparent glass capillary in the nanofluid while the differential interferometry technique was used to study the interactions of the oil meniscus with the wall (glass substrate) in the presence of the nanofluid.

2.2. Materials and preparation of solutions

2.2.1. Oil

Two different oils were used in our experiments: hexadecane and jojoba oil. Hexadecane is a model system suitable for fundamental study while jojoba oil is a natural product. Hexadecane (minimum 99% in purity) was purchased from Sigma–Aldrich. Jojoba oil (100% pure) was obtained from The Jojoba Company. A small amount (<100 ppm) of fat red 7B dye (Sigma, St. Louis, MO) was added to the oil phase to increase the contrast in order to better visually monitor the oil film dewetting process inside the glass capillary.

2.2.2. Nanofluids

2.2.2.1. Silica nanofluid. A colloidal dispersion of silicon(IV) oxide in water (40 wt%, Alfa Aesar) was diluted with DI water to prepare the 10 vol% silica nanofluid that had a 20 nm nominal (geometric) diameter with a density of 1.15 g/cm^3 and pH of 9.7. A small amount of sodium dodecyl sulfate (SDS, VWR Scientific (USA), 5 mM) was added to the solution. SDS was used below the CMC to reduce the contact angle in order to better help the oil film formation on the capillary wall. The silica nanofluid was used since it is commercially available and environmentally friendly [64].

2.2.2.2. Polymer nanofluid. Since the silica nanofluid is sensitive to the electrolyte (a common situation often encountered in oil recovery), it will be unstable and aggregate. In this case, a more stable nanofluid is needed. Since the polymer is not sensitive to brine, we used it to prepare the polymer nanofluid. The polymer nanofluid was prepared by dissolving 0.27 wt% polyethylene glycol 8000 (PEG 8000, Fisher Scientific, USA) and 5 mM SDS in water.

2.2.2.3. Silica nanofluid in glycerol. A colloidal dispersion of silicon(IV) oxide in water (40 wt%, Alfa Aesar) was diluted with the same volume of glycerol to prepare 10 v% silica nanofluid in glycerol.

2.2.3. Glass capillary

The glass capillary was purchased from Cole-Parmer (USA). We measured the inner diameter (ID) at different points by optical microscopy instead of using the manufacturer's quoted value. We randomly chose a few capillaries and found no significant differences between the measurements at various points. The measured

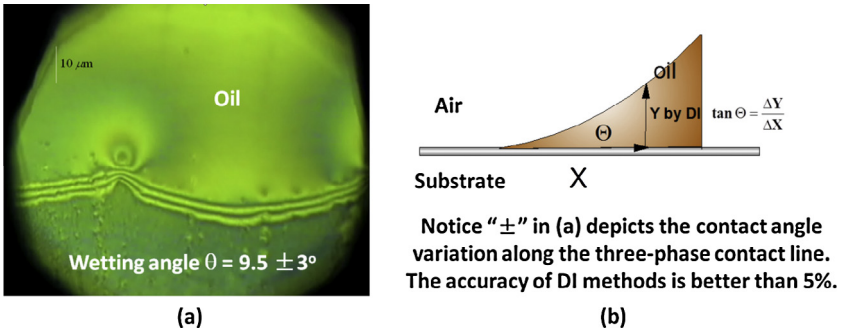

Fig. 5. Three-phase contact angle of crude oil wetting glass using the differential interferometric technique. (a) Interferogram; (b) sketch of principle.

inner diameter is 282 ± 2 μm. Each sample was used only once and discarded after the measurement. Reproducible results were thus obtained simply by using a new capillary without the need for further surface cleaning.

All reagents were used for all tests without further treatment. Unless otherwise stated, water purified in a Milli-Q water deionizer system was used throughout the experiments.

2.3. Nanofluid characterizations

In order to optimize the nanofluid formulation and enhance the effect of the structural forces on the phenomenon of the nanofluid causing the displacement of oil from the capillary, the nanofluid composition was selected using a multistep process [65].

First, the nanofluid needed have a small nanoparticle size and have a low polydispersity. High polydispersity results in a decreased value for the structural disjoining pressure. For example, Chu et al. indicated that a 20% polydispersity in particle size can result in a 30% decrease in the structural disjoining pressure [66].

Second, the formulated nanofluid should have a high osmotic pressure (e.g., higher than about 200 Pa for a 10 vol% nanofluid). Trokhymchuk et al. [16] developed an analytical expression for the structural disjoining pressure (Π_{st}) based on a solution of the Ornstein–Zernike statistical mechanics equation:

$$\begin{aligned} \Pi_{st}(h) &= -P \quad 0 < h < d \\ \Pi_{st}(h) &= \Pi_0 \cos(\omega h + \varphi_2) e^{-\kappa h} + \Pi_1 e^{-\delta(h-d)} \quad h > d \end{aligned} \tag{1}$$

where d is the diameter of the nanoparticle, h is the wedge film thickness and all other parameters (Π_0, Π_1, ω, φ_2, κ, δ) in Eq. (1) are fitted as cubic polynomials in terms of the nanofluid volume fraction (ϕ). P is the osmotic pressure, which is a function of the nanofluid volume fraction shown in Eq. (2):

Table 1
Properties of different types of nanofluids used in our experiment.

Nanofluid type	Size (nm)	Polydispersity (%)	Osmotic pressure (Pa)	Contact angle (°)
10 v% silica nanofluid in water	20	10.5	278	1.6 ± 0.3
Polymer nanofluid	9	8	860	2.2 ± 0.2
10 v% silica nanofluid in glycerol	20	10.5	252	3.8 ± 0.4

$$P = \rho k T \frac{1 + \phi + \phi^2 - \phi^3}{(1 - \phi)^3} \tag{2}$$

where ρ is the particle number density, k is the Boltzmann constant and T is the temperature. As shown above, the structural disjoining pressure and osmotic pressure increase with the increasing nanoparticle volume fraction. A nanofluid with a high osmotic pressure results in a high structural force.

Third, a nanofluid should have a small solid/nanofluid/oil three-phase contact angle in order to maximize the structural force. Kondiparty et al. [47] showed that a low contact angle aids in the spreading of the nanofluid film on a solid surface by confining the nanoparticles in the film–meniscus region and enhancing the structural force. From Young's equation, we also know that a low oil/nanofluid interfacial tension can decrease the solid/nanofluid/oil three-phase contact angle.

The detailed properties of the nanofluid used in the present study are summarized in Table 1.

2.4. Experimental set-up

2.4.1. Macroscopic optical experimental set-up to capture the meniscus dynamics

The macroscopic experimental set-up is shown in Fig. 6. The glass capillary with an inner diameter of 282 ± 2 μm was partially filled with hexadecane by the capillary rise method and then placed in a specially designed horizontal channel (Fig. 6a and b). A small pit was made on the support plate to place the nanofluid into the capillary. A buffer hole was made on the capillary support plate in order to avoid the movement of the nanofluid to the other side of capillary (thus forming a second meniscus). Hexadecane was displaced quickly when it came in contact with the nanofluid and a thick hexadecane film was formed on the capillary wall (Fig. 6c). The shape of the oil meniscus is concave in the presence of the nanofluid. The dynamics of the thick hexadecane film were monitored using reflected light microscopy and a digital camera (Canon PowerShot A720 IS) equipped with a 58 mm macro lens. The camera was used to record the hexadecane film stability when hexadecane was displaced by the nanofluid.

2.4.2. Microscopic experiment setup to monitor meniscus interaction with the glass substrate

The interaction of the meniscus and glass substrate was studied using the reflected light differential interferometry technique. A

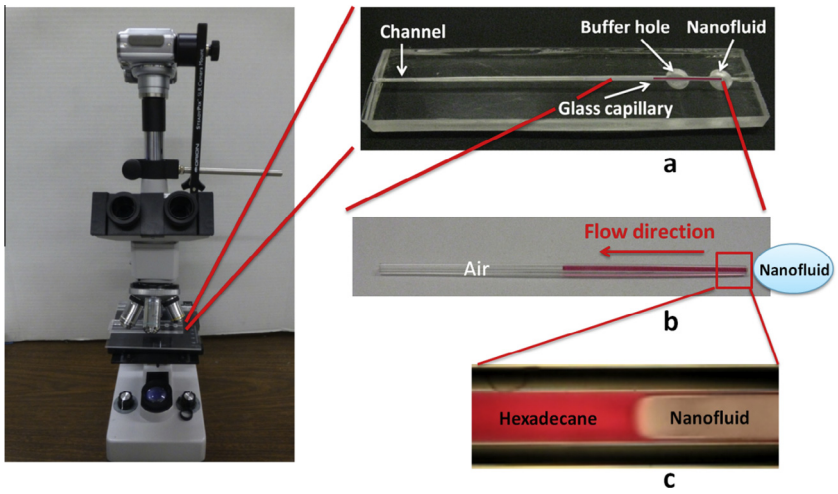

Fig. 6. The optical set-up used to monitor the hexadecane film dewetting dynamics in a horizontal glass capillary in the nanofluid at 25 °C. (a) Magnified horizontal channel with a glass capillary in it; (b) glass capillary partially filled with hexadecane; (c) the shape of the hexadecane meniscus in the presence of the nanofluid.[28].

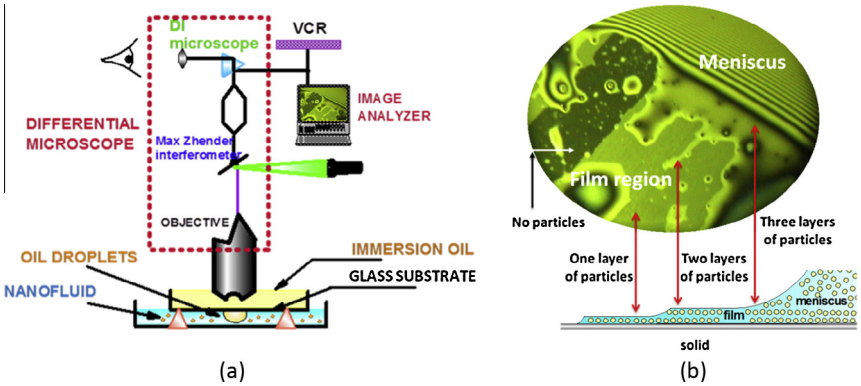

Fig. 7. (a) Schematic of the optical arrangement for studying the solid-nanofluid-oil meniscus interactions; (b) photomicrograph depicting the particle layering of 10 v% silica nanoparticles on a solid surface.

sketch of the optical arrangement is shown in Fig. 7(a). Detailed procedures can be found in Ref. [46]. Basically, a drop of oil expelled into the nanofluid in the cell approaches an optically smooth glass surface, forming a nanofluid film. In the reflected light mode of the microscope, monochromatic light through the top of the glass cell is incident on the film surface. As the nanofluid film between the oil drop and the glass surface thins, the film thickness changes, producing interference patterns (Fig. 7(b)). The high-resolution CCD camera records the process of film thinning.

3. Results and discussion

The role of the nanofluid on the capillary phenomenon has been explored both theoretically and experimentally, especially in the area of wetting and spreading with a nanofluid [44–50,67–72]. The mechanism of the nanofluid-enhanced wetting is still not completely understood. Miller and Ruckenstein [73] proposed slip velocity wetting driven by the surface forces gradient and Shanahan [74,75] proposed a model considering the condensation transport on the wetting dynamics due to the increase in the meniscus curvature effect near the contact line. The phenomena of nanofluid ordering in a wedge film and a solid with wetting driven by the film tension gradient were elucidated by Wasan and Nikolov [44–50], and Sefiane et al. [67,68]. A more recent review of this area can be found in Ref. [37]. In addition, significant research has explored the capillary-driven flow using nanofluids in porous media [28,65,76–81]. Most of these studies focus on the exploration for enhanced oil recovery with nanofluids. Little work has been done on how the nanofluids influence the flow inside the capillary and dynamics of the oil meniscus in the presence of a nanofluid. Here, we would like to discuss one example of the capillary-driven phenomenon in the presence of the nanofluid.

3.1. Observations

3.1.1. Hexadecane film dynamics inside a glass capillary in a silica nanofluid from the macroscopic optical technique

A sequence of photos showing the hexadecane film dewetting process is depicted in Fig. 8.

Initially, the glass capillary was partially filled with hexadecane. After introducing the silica nanofluid, the hexadecane was displaced quickly when it came in contact with the silica nanofluid. This occurred because the capillary pressures at the two sides (one side is hexadecane/silica nanofluid and the other side is hexadecane/air) are different and a thick hexadecane film is formed on the capillary wall. Over time, the thickness of the oil film on the capillary wall fluctuates, and the film becomes unstable and rup-

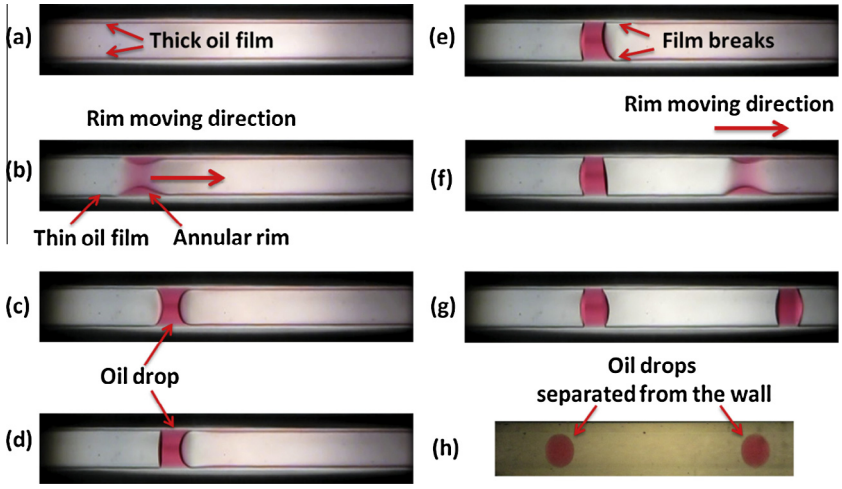

Fig. 8. Evolution of the hexadecane film inside the glass capillary (ID = 282 ± 2 μm) in the silica nanofluid. (a) A thick film was left on the capillary wall after the hexadecane was displaced by the silica nanofluid; (b) dewetting occurs in the form of the annular rim collecting liquid; (c) the annular rim forms a double concave meniscus across the capillary; (d) the thin film ruptures on the right side of the meniscus and the contact angle increases to around 90°; (e–g) repeats the previous steps and forms a second oil drop; (h) oil drops are separated from the capillary wall by the nanofluid.

tures due to the Rayleigh instability. Once it breaks up, it retracts from the capillary wall by the formation of an annular rim. The rim is moving in the direction of the thick film. As the rim moves, it collects liquid from the capillary wall and its volume increases with time; in the later stage, the annular shape becomes unstable and suddenly forms a double concave meniscus across the capillary, causing the dewetting to stop. The contact angle on the right side of the double concave meniscus increases to around 90°. The process then repeats until oil droplets build up all along the glass capillary. Finally, the droplets are displaced from the capillary wall by the silica nanofluid and form spherical droplets inside the capillary by the structural disjoining pressure created on the capillary wall due to the nanoparticles' structuring in the wedge region. Video Clip 1 (see the Supporting Information) depicts the whole process of the hexadecane film dewetting dynamics inside of a glass capillary when hexadecane is displaced by the nanofluid.

The exact same phenomenon was also observed when we used the other two systems: hexadecane/polymer nanofluid and jojoba oil/silica nanofluid in glycerol. Video Clips 2 and 3 (see the Supporting Information) show the whole process using these two nanofluids.

A control experiment in which we use the reference solution (5 mM SDS in water) was also conducted. In this case, we did not observe film formation after hexadecane was displaced by the reference. Video Clip 4 (see the Supporting Information) depicts the entire process.

In order to understand how the nanofluid interacts with the glass capillary wall, we need to conduct a microscopic study with the differential interferometry technique.

3.1.2. Laying of the nanofluidic film on a solid substrate probed by the differential interferometry technique

Initially, the oil droplet separated by the aqueous nanofluid film rolls under the glass surface. Video Clip 5 (see the Supporting Information) shows the various stages of the thinning of the aqueous nanofluid film between the oil droplet and the glass surface. Fig. 7b shows a photomicrograph depicting four different particle structural transitions inside the nanofluid film. The dark green[1] color contains three particle layers; a bright green color contains two particle layers; a green color indicates one particle layer, and a dark color means a film without any particles inside it. From the interference pattern, we can also obtain the thickness of the film with different layers of nanoparticle and nanofluid film-oil meniscus microscopic contact angle, and thereby the structural interaction energy between the film surfaces with the Frumkin–Derjaguin equation. Interested readers can refer to Refs. [46,82,83] on the details of how to get each of these.

Since we have the microscopic explanation of how the nanofluid interacts with the wall, we now go back to the macroscopic approach and analyze the meniscus movement inside the capillary.

3.1.3. Experimental rim velocity

The rim velocity was calculated directly from the experimental observation by monitoring the distance vs. time.

3.1.3.1. Experimental rim velocity in the silica nanofluid. Fig. 9 shows the annular rim moving distance as a function of time in silica nanofluid. From Fig. 9, we can see the rim moving velocity is constant with time, 0.14 ± 0.02 cm/s.

3.1.3.2. Experimental rim velocity in the polymer nanofluid. Fig. 10 shows the annular rim moving distance as a function of time in the polymer nanofluid. The experimentally measured rim velocity is 985 ± 46 μm/s.

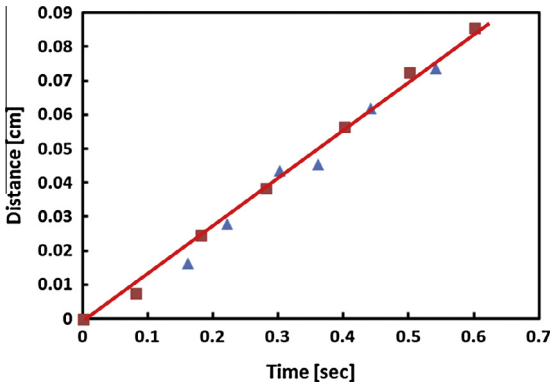

Fig. 9. Rim moving distance as a function of time in the silica nanofluid. The different symbols (■, ▲) correspond to the two repeating sequences in Video Clip 1 in the Supporting Information.

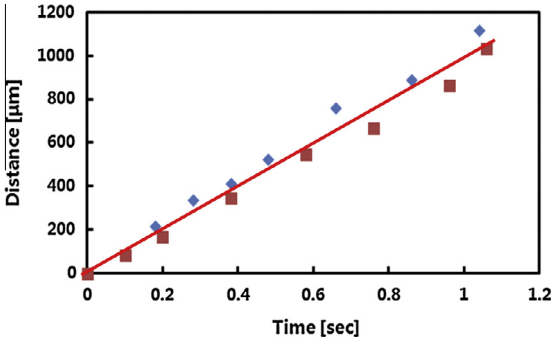

Fig. 10. Rim moving distance as a function of time in the polymer nanofluid. The different symbols (■, ◆) correspond to the two repeating sequences in Video Clip 2 in the Supporting Information.

3.1.3.3. Experimental rim velocity in the silica nanofluid in glycerol. Fig. 11 shows the annular rim moving distance as a function of time in the silica nanofluid in glycerol. The dewetting velocity in this case is 48 ± 6 μm/s.

3.2. Modeling

3.2.1. Model of the oil film's dewetting velocity inside the glass capillary in the nanofluid

Callegari et al. [39] developed a theoretical model describing the annular rim moving velocity inside the nonwettable capillary (liquid does not "like" to wet). In their paper, the rim velocity they derived is given in Eq. (3):

$$V_d = \frac{\theta_E}{\eta l_n}\left(|S| + \frac{e^2}{2b(b-e)}\gamma\right) \tag{3}$$

where θ_E is the equilibrium contact angle between the rim and wall, η is the hexadecane viscosity, l_n is a logarithmic factor that describes the divergence of the viscous dissipation in the two liquid wedges and the value ranges from 6 to 20, b is the capillary radius, e is the thickness of the hexadecane film, S is the spreading coefficient $|S| = \gamma(1 - \cos\theta_E)$, and γ is the interfacial tension between hexadecane and the nanofluid. However, they did not provide experimental data to validate their model; in addition, the dewetting velocity in their model contains a logarithmic factor that describes the diver-

[1] For interpretation of color in Fig. 7, the reader is referred to the web version of this article.

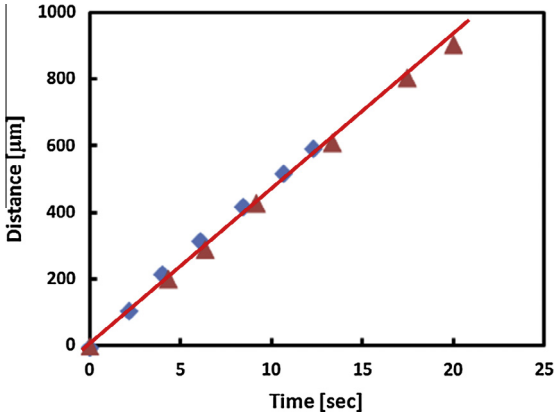

Fig. 11. Rim moving distance as a function of time in the silica nanofluid in glycerol. The different symbols (▲, ◆) correspond to the two repeating sequences in Video Clip 3 in the Supporting Information.

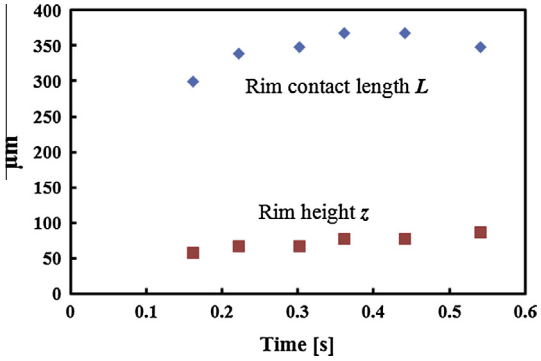

Fig. 13. Rim contact length L and rim height z vs. time.

gence of the viscous dissipation in the two liquid wedges, so it is difficult to assess its exact value.

We recently [28] developed a theoretical model based on the lubrication approximation using the capillary pressure gradient as the driving force to estimate the rim velocity. The rim's moving velocity, U, is shown in Eq. (4)

$$U = \frac{2zh_1\gamma}{\mu L}\left(\frac{1}{b-h_2} - \frac{\cos\theta}{b-h_1}\right) \tag{4}$$

where z is the annular rim height, h_1 is the thickness of the thin hexadecane film, γ is the hexadecane/nanofluid interfacial tension, μ is the hexadecane viscosity, L is the contact length between the rim and capillary wall, θ is the contact angle between the rear meniscus and thin film, b is the capillary radius, and h_2 is the thickness of the thick hexadecane film. We also did experiments with a micellar nanofluid (0.03 mol/L SDS in water) in two different sizes of glass capillary, measured the experimental rim velocity, and then compared these results with the predictions from the model. The predictions from this model are found to be in fair agreement with the experimentally measured values.

We then used the Eq. (4) to predict the rim velocity. Since the phenomenon was the same for all three systems, we report here the detailed analyzed data of hexadecane dewetting dynamics in a silica nanofluid.

As seen from Eq. (4), in order to predict the dewetting velocity, we need to know the film thicknesses h_1 and h_2, rim meniscus, thin film contact angle θ, rim height z, and contact length L. We discuss below how we estimated each of these parameters in Eq. (4).

3.2.2. Rim velocity prediction

3.2.2.1. Film thickness (h_1 and h_2) estimation. Based on the observation that the rim is sliding over a thin film (this is shown in Video Clip 1 and Fig. 8c and d), the dewetting stops when the liquid rim forms a double concave meniscus. Over time, the contact angle on the right side increases—the thin film ruptures—indicating a film is left behind when the rim is moving. Since the capillary number, $Ca = \mu U/\gamma$, is estimated to be 6.1×10^{-4} (much less than 1), the lubrication thin-film thickness h_1 can be estimated using Landau and Levich's lubrication approach for the deep coating model. [23,29]

$$\frac{h_1}{b} = 0.643(6Ca)^{2/3} \tag{5}$$

The thickness of a thick film can be estimated indirectly from the volume conservation. From the photographs in Fig. 12a and b, the volume of the cylindrical drop can be approximated by $V = \pi b^2 l_1$ and can also be expressed as $2\pi b l_2(h_2 - h_1)$, which is the volume of the liquid collected from the thick film; thus, the difference between the thick film and thin film is

$$h_2 - h_1 = \frac{bl_1}{2l_2} \tag{6}$$

where b is the capillary radius, l_1 is the width of the cylindrical drop, and l_2 is the distance between two adjacent cylindrical droplets. After substituting all the quantities into Eqs. (5) and (6), we can calculate that the thin-film thickness is $h_1 = 2.2 \pm 0.3$ μm and the thick-film thickness is $h_2 = 12.5 \pm 0.3$ μm.

3.2.2.2. Contact angle (θ) estimation. In this case, since the thin film thickness at the rear part of the rim is around 2.2 μm, the contact angle of the meniscus and the thin film is very small, practically zero. In our estimation of the rim velocity, we use a contact angle that is zero.

3.2.2.3. Rim contact length L and rim height z. We measured the rim contact length and rim height directly from the experiment at different times. Since the rim is moving, it collects oil from the capillary wall and its volume increases over time. Fig. 13 shows the contact length and rim height vs. time. As can be seen from Fig. 13, the contact length first increases almost linearly with time and then decreases a little at a later stage when the annular rim forms the double concave meniscus. The rim height increases until the annular rim becomes a double concave meniscus. Although the contact length and height increase with time, the ratio of z/L is

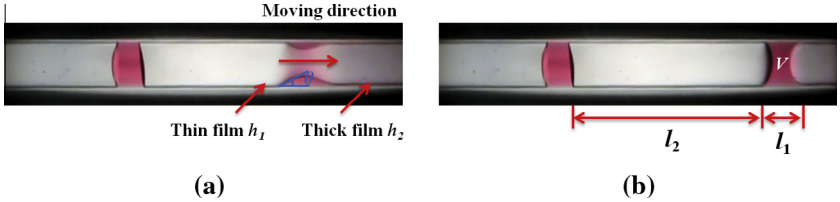

Fig. 12. (a) Annular rim collecting liquid; (b) annular rim becomes a cylindrical drop across the capillary.

Table 2
Experimental vs. predicted rim moving velocity inside the glass capillary (ID = 282 ± 2 μm) in various systems.

Systems	Experimental velocity	Model prediction
Hexadecane/silica nanofluid	0.14 ± 0.02 cm/s	0.11–0.16 cm/s
Hexadecane/polymer nanofluid	985 ± 46 μm/s	880–1090 μm/s
Jojoba oil/silica nanofluid in glycerol	48 ± 6 μm/s	44–64 μm/s
Hexadecane/SDS micellar nanofluid [28]	451 ± 30 μm/s	320–440 μm/s

almost constant, around 0.21 ± 0.02; this can be seen in Fig. 13, which shows that the slopes of the two curves are similar.

3.2.2.4. Comparison of the model prediction with the experiment. Since we have already estimated all the parameters needed to solve Eq. (4), we can then calculate the rim moving velocity using this equation. The prediction of the rim velocity is around 0.11–0.16 cm/s, and can be compared with the experimentally measured value of 0.14 ± 0.02 cm/s in a capillary with an ID = 282 ± 2 μm. The velocity predicted from the present model is in fair agreement with our experimentally observed value.

We repeated the same steps and analyzed data for the other two systems; the results are summarized in Table 2. Table 2 lists the different systems used, experimentally measured rim velocity, and predicted velocity from the model.

As we can see from Table 2, in each case, the present model gives a fair prediction of the experimental results.

4. Conclusions

In summary, we reviewed the capillary-driven phenomena in the capillary and the experimental methods used to visualize the meniscus in the literature. We used a transmitted light microscope to monitor the dynamics of the meniscus. The meniscus dynamics were studied using three different oil/nanofluid systems. We also predicted the meniscus velocity using our recently developed model in each case. The predicted velocities are in fair agreement with the experimentally measured values. To have a microscopic understanding of how the nanofluid interacts with the wall, we employed the differential interferometry technique. We found that nanoparticles tend to self-structure into multiple layers parallel to the solid wall; as a result, the film reduces its thickness in a stepwise manner by stratification. The microscopic study aids our understanding of the macroscopic observations of meniscus dynamics in a nanofluid, especially in the last stage—oil drops were displaced from the capillary wall by the nanofluid.

This study is widely applicable in practical systems (like oil recovery from porous media using a nanofluid, microfluidics, and nanofluidics), and the present model can be used to predict the meniscus velocity in the presence of another immiscible liquid from its cylindrical geometry.

5. Outlook for the future

Despite the plethora of studies in the literature, additional work needs to be done to better understand the dynamics of nanofluid spreading, wetting solids, bubble-meniscus dynamics, and oily phase displacement from the capillary. These studies include:

1. Experiments should be conducted on nanofluid wetting, its spreading on substrates and the oily phases displacement on a capillary wall with different wettabilities (such as a hydrophobic capillary like PVC) in order to develop new methods and progresses.
2. The nanofluid's structural forces depend on the nanofluid's size, shape, concentration, polydispersity, film thickness, and nature of the substrate's surface. The effect of these parameters on the nanofluid wetting–dewetting phenomena should be elucidated.
3. The dynamics of wetting–dewetting solids by a nanofluid and the wetting film's stability mechanisms require more study and better understanding.
4. Simulations and theoretical studies of the oil film dynamics in a nanofluid need to be conducted to improve our understanding of the role of the structural forces on the separation of oil from the capillary wall.

Resolving these issues through scientific rigor and careful experimentation will enhance the potential applications of nanofluids, including their potential use as a "green technology" for enhancing petroleum recovery from reservoirs.

Appendix A. Supplementary material

Supplementary data associated with this article can be found, in the online version, at http://dx.doi.org/10.1016/j.jcis.2014.10.057.

References

[1] R. Lucas, Kolloid Z. 23 (1918) 15–22.
[2] E.W. Washburn, Phys. Rev. 17 (1921) 273–283.
[3] E.K. Rideal, Phil. Mag. 44 (1922) 1152–1159.
[4] F.P. Bretherton, J. Fluid Mech. 10 (1961) 166–188.
[5] A. Griffiths, Proc. Phys. Soc. London 23 (1910) 190–197.
[6] G. Taylor, Proc. R. Soc. Lond. A 219 (1953) 186–203.
[7] G. Taylor, Proc. R. Soc. Lond. A 225 (1954) 473–477.
[8] A.J. Goldman, R.G. Cox, H. Brenner, Chem. Eng. Sci. 22 (1967) 637–651.
[9] I. Frankel, H. Brenner, J. Fluid Mech. 204 (1989) 97–119.
[10] H. Brenner, D.A. Edwards, Macrotransport Processes, Butterworth-Heinemann, Boston, MA, 1993.
[11] K.D. Dorfman, H. Brenner, Phys. Rev. E 65 (2002) 021103.
[12] S. Supple, N. Quirke, Phys. Rev. Lett. 90 (2003) 214501.
[13] E.M. Kotsalis, J.H. Walther, P. Koumoutsakos, Int. J. Multiphase Flow 30 (2004) 995–1010.
[14] M. Majumder, N. Chopra, R. Andrews, B.J. Hinds, Nature 438 (2005) 44.
[15] M. Whitby, N. Quirke, Nat. Nanotechnol. 2 (2007) 87–94.
[16] A. Trokhymchuk, D. Henderson, A.D. Nikolov, D.T. Wasan, Langmuir 17 (2001) 4940–4947.
[17] A. Trokhymchuk, D. Henderson, A. Nikolov, D.T. Wasan, Langmuir 20 (2004) 7036–7044.
[18] D. Henderson, A. Trokhymchuk, A. Nikolov, D.T. Wasan, Ind. Eng. Chem. Res. 44 (2005) 1175–1180.
[19] A. Trokhymchuk, D. Henderson, A. Nikolov, D.T. Wasan, Langmuir 21 (2005) 10240–10250.
[20] J.S. Vesaratchanon, A. Nikolov, D.T. Wasan, D. Henderson, Ind. Eng. Chem. Res. 48 (2009) 6641–6651.
[21] R.N. Marchessault, S.G. Mason, Ind. Eng. Chem. 52 (1960) 79–84.
[22] H.L. Goldsmith, S.G. Mason, J. Colloid Sci. 18 (1963) 237–261.
[23] L. Landau, B. Levich, Acta Physicochim. URSS 17 (1942) 42–54.
[24] V. Levich, Physicochemical Hydrodynamics, Prentice Hall Inc., 1962.
[25] B.V Deryagin, S.M Levi, Film Coating Theory, Focal Press, 1964. December.
[26] S.D.R. Wilson, J. Eng. Math. 16 (1982) 209–221.
[27] K.J. Ruschak, Ann. Rev. Fluid Mech. 17 (1985) 65–89.
[28] H. Zhang, A.D. Nikolov, D.T. Wasan, Langmuir 30 (2014) 9430–9435.
[29] R.F. Probstein, Physicochemical Hydrodynamics: An Introduction, second ed., Wiley, New York, 1994.
[30] P.-G. de Gennes, F. Brochard-Wyart, D. Quere, Capillarity and Wetting Phenomena: Drops, Bubbles, Pearls, Waves, Springer, New York, 2003.
[31] S. Middleman, Modeling Axisymmetric Flows: Dynamics of Films, Jets, and Drops, Academic Press, 1995.
[32] A. Frumkin, Zh. Fiz. Khim. 12 (1938) 337 (in Russian).
[33] B. Derjaguin, Zh. Fiz. Khim. 14 (1940) 137 (in Russian).
[34] A. Scheludko, Proc. Kon. Ned. Akad. Wet. B 65 (1962) 86.
[35] A. Vrij, Discuss. Faraday Soc. 42 (1966) 23–33.
[36] D. Edwards, H. Brenner, D.T. Wasan, Interfacial Transport Processes and Rheology, Butterworth-Heinemann, Boston, MA, 1991.
[37] A. Nikolov, D.T. Wasan, Adv. Colloid Interface Sci. 206 (2014) 207–221.
[38] D.J. Henderson, A.D. Nikolov, A. Trokhymchuk, D.T. Wasan, Confinement-induced structural forces in colloidal systems, in: P. Somasundaran (Ed.), Encyclopedia of Surface and Colloid Science, second ed., Taylor and Francis, New York, 2006.
[39] G. Callegari, A. Calvo, J.P. Hulin, J.P. Hulin, F. Brochard-Wyart, Langmuir 18 (2002) 4795–4798.

[40] G. Callegari, A. Calvo, J.P. Hulin, Eur. Phys. J. E 16 (2005) 283–290.
[41] K.L. Mittal, In Contact Angle, Wettability and Adhesion, vol. 4, American Chemical Society, Washington, DC, 2006. pp. 29–41.
[42] V. Bergeron, A.I. Jimenez-Laguna, C.J. Radke, Langmuir 8 (1992) 3027–3032.
[43] R.W. Aul, W.L. Olbricht, J. Fluid Mech. 215 (1990) 585–599.
[44] D.T. Wasan, A.D. Nikolov, Nature 423 (2003) 156–159.
[45] A. Chengara, A.D. Nikolov, D.T. Wasan, A. Trokhymchuk, D. Henderson, J. Colloid Interface Sci. 280 (2004) 192–201.
[46] A.D. Nikolov, K. Kondiparty, D.T. Wasan, Langmuir 26 (2010) 7665–7670.
[47] K. Kondiparty, A.D. Nikolov, S. Wu, D.T. Wasan, Langmuir 27 (2011) 3324–3335.
[48] K. Kondiparty, A.D. Nikolov, S. Wu, D.T. Wasan, K. Liu, Langmuir 28 (2012) 14618–14623.
[49] K. Liu, K. Kondiparty, A.D. Nikolov, D.T. Wasan, Langmuir 28 (2012) 16274–16284.
[50] S. Wu, A.D. Nikolov, D.T. Wasan, J. Colloid Interface Sci. 396 (2013) 293–306.
[51] M. Cachile, R. Chertcoff, A. Calvo, et al., J. Colloid Interface Sci. 182 (1996) 483–491.
[52] J. Sung, Y.B. Kim, M.H. Lee, Transient phenomena of dynamic contact angle in microcapillary flow, in: 15th International Symposium on Flow Visualization, Minsk, Belarus, June 25–28, 2012.
[53] T. Andrukh, D. Monaenkova, B. Rubin, et al., Soft Matter. 10 (2014) 609–615.
[54] A.T. Paxson, K.K. Varanasi, Nat. Commun. 4 (2013) 1492.
[55] P. Papadopoulos, L. Mammen, X. Deng, et al., PNAS 110 (2013) 3254–3258.
[56] S. Moulinet, D. Bartolo, Eur. Phys. J. E 24 (2007) 251–260.
[57] C. Antonini, J.B. Lee, T. Maitra, et al., Sci. Rep. 4 (2014) 4055. http://dx.doi.org/10.1038/srep04055.
[58] A.D. Nikolov, P.A. Kralchevsky, I.B. Ivanov, J. Colloid Interface Sci. 112 (1986) 122–131.
[59] A.D. Nikolov, P.A. Kralchevsky, I.B. Ivanov, A.S. Dimitrov, AIChE Symp. Ser. 252 (82) (1986) 82–90.
[60] A.D. Nikolov, A.S. Dimitrov, P.A. Kralchevsky, Opt. Acta 33 (1986) 1359–1386.
[61] A.M. Cazabat, F. Heslot, S.M. Troian, P. Carles, Nature 346 (1990) 824–826.
[62] A.S. Dimitrov, P.A. Kralchevsky, A.D. Nikolov, D.T. Wasan, Colloids Surf. 47 (1990) 299–321.
[63] R. Bassani, E. Ciulli, Lubricant film thickness and shape using interferometry and image processing, in: D. Dowson et al. (Eds.), Proc. 23rd Leeds-Lyon Symp. on Trib, Elsevier, 1997, pp. 81–90.
[64] G. Ramesh, N.K. Prabhu, Nanoscale Res. Lett. 6 (2011) 334–348.
[65] H. Zhang, A.D. Nikolov, D.T. Wasan, Energy Fuels 28 (2014) 3002–3009.
[66] X.L. Chu, A.D. Nikolov, D.T. Wasan, Langmuir 12 (1996) 5004–5010.
[67] K. Sefiane, J. Skilling, J. MacGillivray, Adv. Colloid Interface Sci. 138 (2008) 101–120.
[68] K. Sefiane, Appl. Phys. Lett. 89 (2006) 044106.
[69] K. Sefiane, R. Bennacer, Adv. Colloid Interface Sci. 147–148 (2009) 263–271.
[70] R.V. Craster, O.K. Matar, K. Sefiane, Langmuir 25 (2009) 3601–3609.
[71] S. Vafaei, T. Borca-Tasciuc, M.Z. Podowski, A. Purkayastha, G. Ramanath, P.M. Ajayan, Nanotechnology 17 (2006) 2523–2527.
[72] S. Vafaei, D. Wen, Microfluid. Nanofluid. 8 (2010) 843–848.
[73] C.A. Miller, E. Ruckenstein, J. Colloid Interface Sci. 48 (1974) 368–373.
[74] M.E.R. Shanahan, Langmuir 17 (2001) 3997–4002.
[75] M.E.R. Shanahan, Langmuir 17 (2001) 8229–8235.
[76] T. Babadagli, J. Colloid Interface Sci. 246 (2002) 203–213.
[77] A. Karimi, Z. Fakhroueian, A. Bahramian, N.P. Khiabani, J.B. Darabad, R. Azin, S. Arya, Energy Fuels 26 (2012) 1028–1036.
[78] M.O. Onyekonwu, N.A. Ogolo, Investigating the use of nanoparticles in enhancing oil recovery, Society for Petroleum Engineers (SPE) Conference Paper SPE-140744-MS, 2010, <http://dx.doi.org/10.2118/140744-MS>.
[79] A. Shahrabadi, H. Bagherzadeh, A. Roustaei, H. Golghanddashti, Experimental investigation of HLP nanofluid potential to enhance oil recovery: a mechanistic approach, Society for Petroleum Engineers (SPE) Conference Paper SPE-156642-MS, 2012, <http://dx.doi.org/10.2118/156642-MS>.
[80] O. Torsater, S. Li, L. Hendraningrat, A coreflood investigation of nanofluid enhanced oil recovery in low-medium permeability berea sandstone, Society for Petroleum Engineers (SPE) Conference Paper SPE-164106-MS, 2012, <http://dx.doi.org/10.2118/164106-MS>.
[81] O. Torsater, S. Li, L. Hendraningrat, Enhancing oil recovery of low-permeability berea sandstone through optimised nanofluids concentration, Society for Petroleum Engineers (SPE) Conference Paper SPE-165283-MS, 2012, <http://dx.doi.org/10.2118/165283-MS>.
[82] A.D. Nikolov, D.T. Wasan, J. Colloid Interface Sci. 133 (1989) 1–12.
[83] A.D. Nikolov, D.T. Wasan, Langmuir 8 (1992) 2985–2994.